

MORDA: A Synthetic Dataset to Facilitate Adaptation of Object Detectors to Unseen Real-target Domain While Preserving Performance on Real-source Domain

Hojun Lim*, Heecheol Yoo*, Jinwoo Lee, Seungmin Jeon, Hyeongseok Jeon†

Abstract—Deep neural network (DNN) based perception models are indispensable in the development of autonomous vehicles (AVs). However, their reliance on large-scale, high-quality data is broadly recognized as a burdensome necessity due to the substantial cost of data acquisition and labeling. Further, the issue is not a one-time concern as AVs might need a new dataset if they are to be deployed to another region (real-target domain) that the in-hand dataset within the real-source domain cannot incorporate. To mitigate this burden, we propose leveraging synthetic environments as an auxiliary domain where the characteristics of real domains are reproduced. This approach could enable indirect experience about the real-target domain in a time- and cost-effective manner. As a practical demonstration of our methodology, nuScenes and South Korea are employed to represent real-source and real-target domains, respectively. That means we construct digital twins for several regions of South Korea, and the data-acquisition framework of nuScenes is reproduced. Blending the aforementioned components within a simulator allows us to obtain a synthetic-fusion domain in which we forge our novel driving dataset, *MORDA: Mixture Of Real-domain characteristics for synthetic-data-assisted Domain Adaptation*. To verify the value of synthetic features that MORDA provides in learning about driving environments of South Korea, 2D/3D detectors are trained solely on a combination of nuScenes and MORDA. Afterward, their performance is evaluated on the unforeseen real-world dataset (AI-Hub¹) collected in South Korea. Our experiments present that MORDA can significantly improve mean Average Precision (mAP) on AI-Hub dataset while that on nuScenes is retained or slightly enhanced. Details on MORDA can be accessed at <https://morda-e8d07e.gitlab.io>.

I. INTRODUCTION

Deep-learning-based techniques have obtained growing attention and have become a major trend in challenging perception tasks of autonomous vehicles (AVs). Such dominance occurs across types of sensor modality: camera [1]–[3], LiDAR [4]–[6], RADAR [7], and even combination of those [8]–[10]. Despite their thrives in AVs, one inherent challenge is the dependency on a large-scale driving dataset. In general, building a dataset for perception tasks involves (1) equipping a car with the desired sensor suite, (2) deploying

* These two authors contributed equally

† Corresponding author

All authors are associated with MORAI Inc., Republic of Korea. Email: {hjlim, hcyoo, jwlee, smjeon, hsjeon}@morai.ai

This research was supported by a grant(code RS-2023-00233952) from R&D Program funded by Ministry of Land, Infrastructure and Transport of Korean government.

¹This research (paper) used datasets from **High-precision data collection vehicle daytime city road data**. All data information can be accessed through **AI-Hub** (<http://www.aihub.or.kr>).

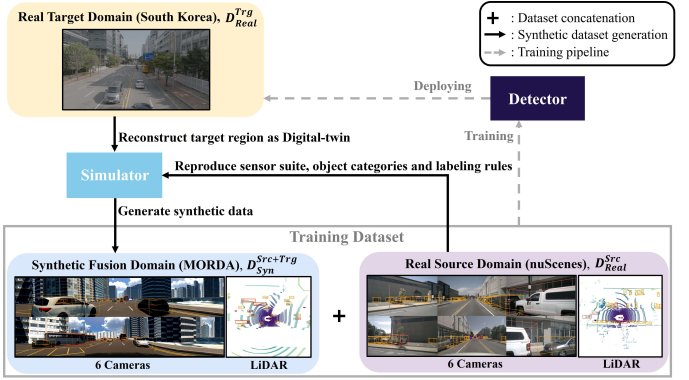


Fig. 1. Research overview: Cost-effective generation of virtual data ($D_{Syn}^{Src+Trg}$) which mimics real-world dataset that one could construct if the sensor configuration of D_{Real}^{Src} were dispatched to the real-target domain D_{Real}^{Trg} . The usefulness of our method is assessed by training object detectors on ($D_{Real}^{Src} + D_{Syn}^{Src+Trg}$) and evaluating on unforeseen D_{Real}^{Trg} .

the car to the regions of interest to collect sensor data, and lastly, (3) generating the ground truth (GT) labels for sensor data according to labeling rules. As widely known, this entire process is time-consuming and cost-heavy.

This challenge gets even more severe when deploying AVs that have been developed for one domain (real-source domain, D_{Real}^{Src}) to another (real-target domain, D_{Real}^{Trg}). In this context, one preferable choice for safety-critical AVs would be rebuilding the training dataset with GT labels for the novel domain. However, this method is indeed pricey.

To alleviate the labeling cost, research on unsupervised domain adaptation (UDA) has been actively conducted. UDA methods assume that only the D_{Real}^{Src} is labeled, and they exploit the knowledge from the annotated D_{Real}^{Src} for better adaptation (i.e., performance) of DNNs to the unlabeled D_{Real}^{Trg} without additional labeling costs [11], [12]. Nevertheless, dispatching the sensor-equipped vehicle to D_{Real}^{Trg} for data collection is inevitable even in this scenario. Further, the engineering cost to synchronize raw data from sensors operating often at different frequencies is non-negligible.

Recently, game engines and simulators have been increasingly employed to reduce the burden given that a large-scale dataset with accurate GT labels can be constructed in a time- and cost-efficient manner [13], [14], [16], [17], [20], [21]. However, many synthetic driving datasets at present are not specifically designed to replicate particular real-world domains, including driving environments, sensor suites, object categories, and labeling policies. Consequently, inconsistencies between those characteristics of real-world

TABLE I
COMPARISON TABLE FOR PROPERTIES REGARDING SENSOR SUITE AND BBOX LABELS ACROSS SYNTHETIC DATASETS.

	Sensor setup				Sensor suite reference	BBox annotation		
	#Camera [*]	Resolution	#LiDAR	#Channel		DOF [†]	Road obstacle [‡]	Frequency(Hz)
VIPER [13]	1	1920×1080	X	X	-	9	X	~15
VKITTI2 [14]	5	1242×375	X	X	KITTI [15]	9	X	-
SYNTHIA-AL [16]	1	640×480	X	X	-	7	X	25
SHIFT [17]	5	1200×800	1	128	-	9	X	10
OPV2V [18]	4	800×600	1	64	-	9	X	10
MORDA (Ours)	6	1600×900	1	32	nuScenes [19]	9	✓	20

(*) Only multi-view cameras are counted, and stereo cameras are not included.
(†) Degree of freedom, 9 means 3D-BBox labels are represented with position (x, y, z), size (length, width, height), and orientation (roll, pitch, yaw). 7 denotes the orientation is represented only with yaw angle.

(‡) Traffic cones and barriers.

(-) Relevant information is not available.

and synthetic datasets might further widen the gap between them, potentially resulting in performance degradation of DNNs when trained on real and synthetic datasets combined.

Given the aforementioned constraints in UDA and existing synthetic datasets, the research objective of this paper is to develop a synthetic dataset that enhances the adaptation of DNNs to D_{Real}^{Trg} while their performance on D_{Real}^{Src} is not degraded. Note that this scenario is challenging as (1) D_{Real}^{Trg} is completely unforeseen, meaning sensor data of the target domain is not used for training DNNs, and (2) the synthetic dataset should improve the generalization ability of DNNs as they need to perform well on both D_{Real}^{Src} and D_{Real}^{Trg} .

We believe an adequate synthetic dataset for our purpose needs to be equipped with the following attributes; (1) Virtual version of geographical features of driving environments in the target domain (D_{Real}^{Trg}), which enables cost-effective indirect exposure of D_{Real}^{Trg} to DNNs. (2) Consistency with D_{Real}^{Src} in terms of sensor suite and labeling process to keep the characteristics of created synthetic dataset paired with D_{Real}^{Src} . In this regard, we propose a methodology to generate a synthetic dataset in a synthetic-fusion domain ($D_{Syn}^{Src+Trg}$) where the mentioned aspects of D_{Real}^{Src} and D_{Real}^{Trg} are well integrated. As a demonstration, we construct a novel synthetic dataset, MORDA which takes nuScenes for D_{Real}^{Src} and South Korea for D_{Real}^{Trg} . Next, we evaluate the efficacy of our MORDA dataset in a challenging scenario, as illustrated in Fig. 1. Firstly, 2D/3D object detectors are trained solely on nuScenes (D_{Real}^{Src}) combined with MORDA ($D_{Syn}^{Src+Trg}$). Afterward, they are evaluated on the unforeseen driving scenes of South Korea (D_{Real}^{Trg}) present in AI-Hub dataset. Our extensive experiments demonstrate that MORDA allows noteworthy detection-performance gain on D_{Real}^{Trg} while successfully maintaining the performance on D_{Real}^{Src} simultaneously. In short, the main contributions are:

- We present MORDA, a synthetic dataset featuring the virtual version of the real driving environments in South Korea and replicating key components of nuScenes in data acquisition and labeling.
- Using MORDA, we show that utilizing $D_{Syn}^{Src+Trg}$ could be a financially-viable method for detectors to adapt to D_{Real}^{Trg} without performance degradation on D_{Real}^{Src} .

II. RELATED WORKS

A. Object Detection

The field of object detection has shown surprising progress with DNNs in recent years, which aims to the accurate

prediction of bounding box (BBox) to localize and classify objects within the sensor’s field-of-view. The prosperity of DNN-based object detection applies to not only 2D but also challenging 3D detection tasks across various sensor modalities [1]–[10]. However, the inherent challenge of learning algorithms remains that the performance degradation occurs when DNNs are evaluated on a new domain which is unforeseen during training [17], [22]. Note that addressing such is imperative for AVs whose driving environments or conditions can often change, e.g., deploying the developed AVs to another country ($D_{Real}^{Src} \rightarrow D_{Real}^{Trg}$).

B. Unsupervised Domain Adaptation (UDA)

To tackle the performance drop in new domains, numerous studies have concentrated on adapting DNNs trained on the source domain (w/ labels) to the target domain (w/o labels). Recent works in this field present notable advances even in challenging LiDAR-based 3D object detection. For example, [11], [12], [23] address the adaptation problem of Waymo [24] → nuScenes [19], presenting notable improvement.

Despite the striving of UDA, several difficulties remain to be resolved. Firstly, adversarial training schemes are often employed to extract domain-invariant features, expecting the learned representations to adapt seamlessly to the target domain [23], [25]. However, as noted in [26], if there is a severe distribution mismatch between source and target domains, it can lead to insufficient generalization. Secondly, sophisticated self-training schemes [11], [12], [27], [28], which leverage knowledge obtained from the labeled source domain to generate pseudo labels for the target domain, naturally risk potential error propagation. Lastly, sensor data collection at the target regions is still required, which could be expensive in practice even without labeling.

C. Synthetic Driving Datasets

Cost-efficient virtual environments have been actively employed to reduce the burden of constructing large-scale driving datasets with rich annotations. For example, Unity² engine is used to generate Virtual KITTI 2 (VKITTI2) [14], and SYNTHIA-AL [16]. A modern game Grand Theft Auto V is utilized to create GTA5 [20] and VIPER [13]. Recently, open-source driving simulator CARLA [29] has been employed to produce SHIFT [17] and OPV2V [18].

Despite prevailing achievements of existing synthetic datasets, they are less suitable for scenarios where their

²<http://unity3d.com>

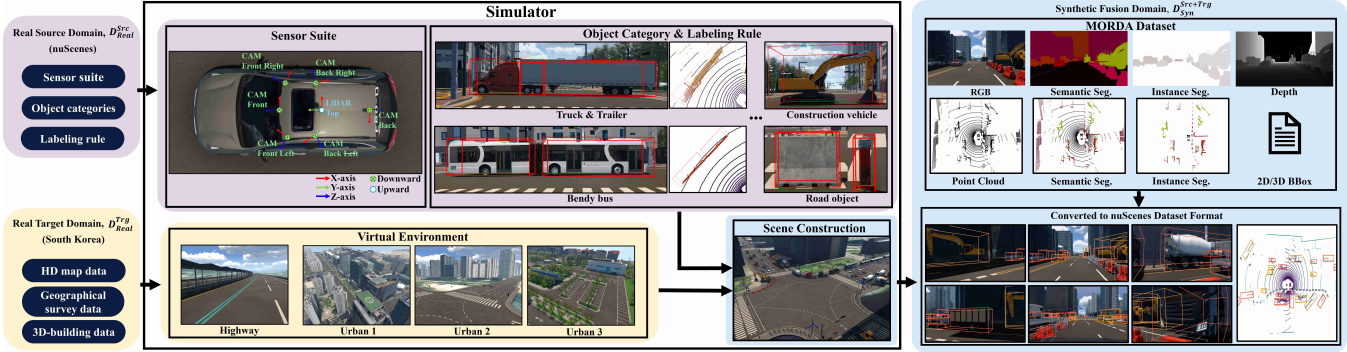


Fig. 2. Architecture of the proposed method to generate MORDA from synthetic-fusion domain ($D_{Syn}^{Src+Trg}$). Digital-twin maps are leveraged to reflect locational features of D_{Real}^{Trg} . Sensor suite and labeling rules from D_{Real}^{Src} are implemented to suppress factors that could cause unexpected discrepancies in data distributions of D_{Real}^{Src} and $D_{Syn}^{Src+Trg}$. Combining both, we ensure $D_{Syn}^{Src+Trg}$ is well aligned with D_{Real}^{Src} and D_{Real}^{Trg} .

role is to assist the adaptation of DNNs trained on D_{Real}^{Src} to unobserved D_{Real}^{Trg} . The reason is that many synthetic datasets are generated from their own sensor suite and virtual worlds with no real-world references. Therefore, there is no guarantee that the geological features of D_{Real}^{Trg} , a target region for deploying AVs with DNNs, are present inside them. VKITTI2 is an exception as it is a digital-version clone of a real-world dataset, KITTI. The mentioned characteristics of VKITTI2 enable it to assess the usefulness of virtual worlds in terms of transferability to the real world. Nevertheless, this validation is limited to camera-related tasks, as LiDAR of KITTI is not implemented in VKITTI2. Furthermore, BBox labels for cyclists and pedestrians that exist in KITTI are absent, which makes it difficult to be used for learning about classes other than vehicles.

Our MORDA dataset benchmarks nuScenes, meaning it incorporates cameras, LiDAR, and 10 detection classes with accurate BBox labels for both modalities. Tab. I compares MORDA with publicly available synthetic datasets.

III. MORDA DATASET GENERATION

A. Overview

The purpose of our method is to construct a dataset from a synthetic-fusion domain ($D_{Syn}^{Src+Trg}$) where DNNs (specifically, 2D/3D object detectors) can indirectly learn about the unforeseen D_{Real}^{Trg} to enhance adaptability while retaining the performance on D_{Real}^{Src} at which the model is trained. To accomplish the aim, we extract pivotal characteristics from D_{Real}^{Src} and D_{Real}^{Trg} . Then, they are reproduced and blended within a simulator, creating our fusion domain. Lastly, our synthetic dataset (MORDA) is generated using the simulator. Fig. 2 illustrates this procedure in detail. As a showcase of the proposed methodology, we choose nuScenes and South Korea to represent D_{Real}^{Src} and D_{Real}^{Trg} , respectively. Next, the MORAI Simulator (MORAI SIM) [30] is employed to provide virtual environment where fundamental features like driving agents and GT-label generation are available.

B. Reproduced Characteristics of Source Domain, D_{Real}^{Src}

We extract three components from D_{Real}^{Src} and implement them in MORAI SIM to create MORDA: sensor suite, list of object categories for detectors to classify, and labeling

rules to draw 3D BBoxes for each category. As nuScenes is employed for D_{Real}^{Src} , its sensor suite (six 1600×900 cameras and one 32-channel spinning LiDAR), object categories (10 detection classes), and annotation rules for 3D BBox are reproduced. The positions and orientations of individual virtual sensors adhere to the configuration of real ones in nuScenes. It is worth mentioning that 3D BBox labeling rules even for complicated categories that have two individual rigid sections (e.g., bendy bus, truck-trailer) are implemented as visualized in Fig. 2. Further, the types of objects used for dataset generation include construction vehicles and road objects (barriers, traffic cones), which are rarely observed in other synthetic datasets at present.

C. Reproduced Characteristics of Target Domain, D_{Real}^{Trg}

We want the geographical features of the real target domain, South Korea, to be reflected in the virtual environment so that our generated MORDA dataset could be enriched with them. To ensure this, we employ four digital-twin maps of South Korea available in MORAI SIM, which consist of one highway and three urban cities. Note that each digital-twin map was constructed upon HD map data, geographical survey data, and 3D building data collected from each counterpointing region in South Korea so that the road surface, terrain, and surrounding static objects can be realistically replicated in the simulator.

D. Data Creation in Synthetic Fusion Domain, $D_{Syn}^{Src+Trg}$

By reproducing the mentioned real-world characteristics in the simulator, we construct $D_{Syn}^{Src+Trg}$, the synthetic-fusion domain where we hypothesize that the features from D_{Real}^{Src} and D_{Real}^{Trg} are appropriately blended. 87 scenes are made in this domain, and for each scene, the ego vehicle drives on a predefined path at a certain place of a digital twin map to collect synthetic sensor data. The scenes are composed of two types: static and dynamic, accounting for 57 and 30.

The major difference between static and dynamic scenes is the presence of moving objects. In static scenes, objects other than the ego vehicle are stationary. However, their arrangement has been meticulously handcrafted to emulate parking lots, construction sites, and road environments filled with huge vehicles. Hence, this type of scene has a larger

number of trucks, trailers, construction vehicles, barriers, and traffic cones than the other type. In contrast to static scenes, the focus of dynamic scenes is to incorporate dense traffic flows with many moving objects into our dataset. To achieve this, we exploit the built-in traffic generator of MORAI SIM, which spawns various agents (e.g., cars and motorcyclists) driving autonomously, to keep the road congested.³

While having the ego vehicle drive in a scene, the synchronized virtual sensors collect data at 20 Hz along with ground-truth (GT) labels. Iterating this process across all scenes yields our MORDA dataset enriched with the simulated geographical features of D_{Real}^{Trg} and object-shape features of D_{Real}^{Src} . Lastly and optionally, we convert MORDA to follow the dataset format of nuScenes. The lower-right corner of Fig. 2 illustrates our converted dataset visualized using nuScenes development toolkit (nuscenes-devkit) [19]. The reason for this conversion is detailed in Sec. V-A.1

IV. MORDA DATASET

A. Dataset Content

MORDA comprises ~37K frames where each frame consists of ego-vehicle pose data, six 1600×900 images, and one 32-channel point cloud data with corresponding GT labels. The types of GT include pixel/point-level semantic and instance segmentation, 2D/3D BBox annotation, and pixel-wise depth values. All types of GT labels are generated independently by individual virtual sensors. Therefore, our dataset can be utilized for various vision tasks such as monocular/multi-view camera-based, lidar-based, fusion-based object detection, and segmentation tasks.

B. Comparison to nuScenes Dataset

MORDA delivers 1.6 million (M) 3D BBox labels for ~37K frames, whereas nuScenes provides 40K frames with 1.4M BBoxes (only keyframes are counted excluding sweeps as they are not annotated). While both datasets present comparable scales of labeled frames, MORDA has ~15% more BBox labels than nuScenes. Furthermore, our dataset presents denser temporal information of objects around ego vehicles as MORDA’s BBox labels are generated at 20 Hz while those of nuScenes are labeled at 2 Hz.

Fig. 3 visualizes the count of 3D BBoxes for each class by dataset. As shown, their distributions largely differ, but MORDA supplements the shortage of 3D BBoxes for several classes in nuScenes. Specifically, the longtailness of rare classes (truck, bus, construction vehicle, trailer, motorcycle, and bicycles) in nuScenes is mitigated when 3D-BBox labels of respective classes in MORDA are concatenated.

Similarly, Fig. 4 depicts the distribution of 2D BBoxes in image space for each dataset where the individual 2D labels are represented as circular markers at coordinates corresponding to their respective widths and heights. In general, the two distributions show a similar tendency and coverage in the width-height 2D space. However, it is noteworthy that

³The traffic flow was set to reach E (operation near or at capacity) or F (breakdown in flow) of Level-of-service (LOS). Details regarding this can be found in [31].

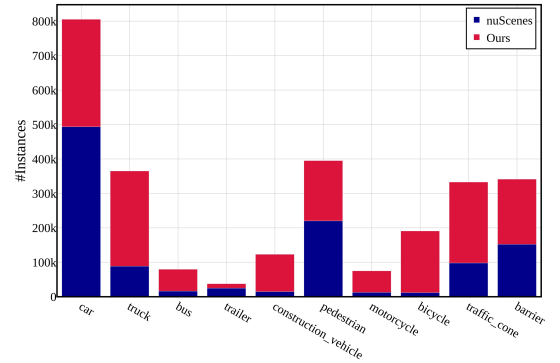


Fig. 3. Distribution of 3D-BBox annotations by category for nuScenes (blue, train + val splits) and MORDA (red).

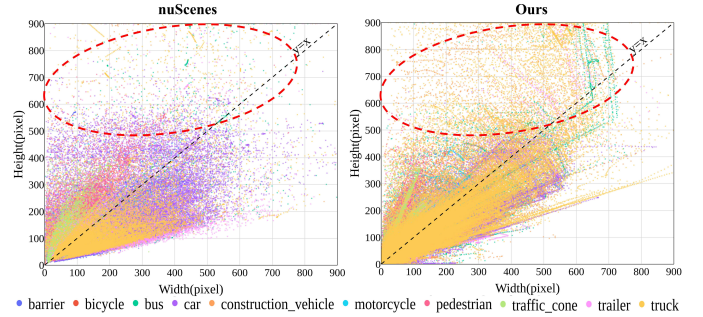


Fig. 4. Scatter plot of 2D-BBox labels for front-camera images in nuScenes (train split) and MORDA. The colors highlight the object category of individual BBox labels. For visibility, the x-axis (width) of plot is clipped at 900 which is the largest value that height of 2D BBox can take. Lastly, BBoxes with area lower or equal to 10 are excluded from visualization.

the distribution of our dataset shows higher density in the area highlighted by the red dotted ellipse where BBox labels with high values for height (500+) and a wide range for width (0 ~ 800) exist. This suggests that images in our dataset contain more diverse shapes of huge vehicles such as buses, construction vehicles, trucks, and trailers, likely at close distances. Combining all the above, mitigation of the class imbalance and enhancement of data diversity could be expected when adding MORDA to nuScenes.

V. EXPERIMENTS

A. Impact of MORDA on D_{Real}^{Src} (nuScenes dataset)

This section presents quantitative results that MORDA could maintain or even improve the performance of camera-based 2D and LiDAR-based 3D detectors on nuScenes.

1) *Pre-processing*: We convert MORDA dataset to follow the format of nuScenes (e.g., structure, file hierarchy, and keyframe-sweep), primarily meaning annotation frequency of MORDA decrease from 20 Hz to 2 Hz. This step is necessary as numerous modern 3D detectors trained on nuScenes, especially LiDAR-based ones, exploit the sweeps (frames w/o annotations) from past time steps for improving point cloud density and robustness of temporal information. Thus, to construct a coherent training environment for those detectors we conduct the format conversion although it decreases the frequency of MORDA (keyframes: ~3.7K, sweeps: ~33K).

TABLE II

QUANTITATIVE EVALUATION OF PERFORMANCE GAIN THAT MORDA ($D_{Syn}^{Src+Trg}$) DELIVERS ON BOTH nuSCENES (D_{Real}^{Src}) AND UNFORESEEN AI-HUB (D_{Real}^{Trg}). C AND L DENOTE CAMERA AND LiDAR, RESPECTIVELY. CV AND MC ARE CONSTRUCTION VEHICLE AND MOTORCYCLE.

Task	Modality	Model	Remark	Training Dataset	Evaluation Dataset													
					nuScenes (D_{Real}^{Src})							AI-Hub (D_{Real}^{Trg})						
					Truck	Bus	Trailer	CV	MC	Bicycle	mAP [†]	NDS	Car	Truck	Bus	Ped	mAP [‡]	
2D	C	Faster-RCNN	✗	nuScenes	31.4	48.0	16.1	4.2	20.9	19.8	27.3	✗	19.5	13.8	16.8	3.3	13.35	✗
2D	C	Faster-RCNN	✗	nuScenes + MORDA	31.0	50.0	16.5	3.7	22.0	20.7	27.8	✗	27.2	18.6	24.5	8.3	19.7	✗
3D	L	PointPillars	SECFPN	nuScenes	39.2	51.7	28.6	5.4	21.5	0.9	34.94	50.02	24.93	3.425	11.70	10.93	12.74	21.95
3D	L	PointPillars	SECFPN	nuScenes + MORDA	40.5	53.1	30.8	7.3	22.9	0.8	35.45	50.44	29.67	5.59	12.28	11.99	14.88	22.63
3D	L	SSN	✗	nuScenes	49.5	65.8	33.7	17.1	52.6	23.3	48.29	59.42	27.30	9.93	19.94	15.48	18.16	26.92
3D	L	SSN	✗	nuScenes + MORDA	52.2	66.4	33.1	16.8	52.5	24.6	48.92	60.41	36.76	13.79	24.16	20.76	23.87	30.21
3D	L	CenterPoint	Pillar (0.2m)	nuScenes	49.0	63.3	31.4	10.9	41.4	18.6	48.96	59.42	0.0*	0.0*	0.065	0.0*	0.016	2.64
3D	L	CenterPoint	Pillar (0.2m)	nuScenes + MORDA	49.5	64.3	32.8	14.3	44.4	13.9	49.43	59.76	14.73	0.012	2.01	0.0*	4.19	11.38
3D	L	CenterPoint	Voxel (0.1m)	nuScenes	53.2	66.5	36.0	15.0	55.2	36.8	56.23	64.51	0.717	0*	0*	0*	0.179	7.203
3D	L	CenterPoint	Voxel (0.1m)	nuScenes + MORDA	55.1	69.2	37.3	18.5	57.0	38.1	57.80	65.47	63.44	5.682	4.264	0*	18.34	22.93
3D	L	CenterPoint	Voxel (0.075m)	nuScenes	55.1	67.9	34.9	15.2	55.8	36.1	56.95	65.40	0.197	0.0*	0.0*	0.0*	0.049	4.19
3D	L	CenterPoint	Voxel (0.075m)	nuScenes + MORDA	55.9	67.1	35.7	16.1	58.4	40.1	58.02	66.02	63.28	1.0	24.6	0.0*	22.22	23.71
					+0.8	-0.8	+0.8	+2.6	+4.0	+1.0	+1.07	+0.62	+63.08	+1.0	+24.6	0.0	+22.17	+19.52

([†]) Over 10 detection classes of nuScenes.

([‡]) Over 4 classes: car, truck, bus, and pedestrian.

(*) If the precision or recall values for all operating points on the precision-recall curve are less than 10%, the AP for that class is set to zero [19].

2) *Training details*: No advanced training or domain-adaptation strategy is applied other than a simple concatenation of nuScenes and MORDA to construct a merged training set. For monocular 2D detection scenario, Faster-RCNN [32] is opted. We employ the implementation of Faster-RCNN from MMDetection [33], and the default training configuration (e.g., learning rate, batch size) remains unchanged. The detector is trained on one RTX 3090 GPU with images that are from the front camera. For LiDAR-based 3D detection, renowned PointPillars [4], SSN [5], and CenterPoint [6] are employed. we use the implementation of the mentioned networks in MMDetection3D [34]. While the other configurations are the same as the default ones, batch size is adjusted to our GPU resources. In short, PointPillars, and SSN are trained on a single RTX 3090 with batch size of 8. CenterPoint is trained on four NVIDIA L4 GPUs with batch sizes set to 8, 8, and 4 for Pillar (0.2m) and Voxel (0.1m, 0.075m), respectively.

3) *Metrics*: We use renowned average precision (AP), mean average precision (mAP), and nuScenes detection score (NDS) [19]. All metrics are represented in percentage (%), and higher scores indicate better performance.

4) *Evaluation*: The left half of Tab. II presents performance of detectors on the validation split of nuScenes. As demonstrated, detectors trained on nuScenes combined with MORDA outperform all baselines that are trained on nuScenes alone in terms of mAP and NDS across modalities and network architectures. While the mAP gains achieved in the other detectors are marginal, MORDA brings notable improvement of 1% to CenterPoint-Voxel (0.1m, 0.075m) models. This gain is worth mentioning as no tailored training strategy was applied to close the sim-to-real gap explicitly.

In addition to mAP, we present class-wise AP for the rare categories that MORDA mitigates long-tail issues discussed in Sec. IV-B. Although the trend of AP improvement or decline varies across models for all six classes, we observe meaningful enhancements, e.g., +2.7% for truck in SSN,

TABLE III
SUMMARY OF PROPERTIES BY DATASET. ARROW(→) INDICATES THE APPLIED PRE-PROCESSING FOR A COHERENT EXPERIMENT SETUP.
T AND V DENOTE TRAIN AND VALIDATION, RESPECTIVELY.

	#Annot.	Frame	#CAM.	Resolution	#Beam	#Det. Class	Freq. (Hz)
nuScenes (T)	28K	6→1		1600×900	32	10	2
MORDA (T)	37K→3.7K	6→1		1600×900	32	10	20→2
AI-Hub (V)	80K→8.8K	5→1		1920×1200→1600×900	128	8→4	10→2

+3.4% and +3.0% for CV and MC in CenterPoint-Pillar, and +4.0% for bicycle in CenterPoint-Voxel(0.075m). Combining all the above leads us to conclude the characteristics of nuScenes we benchmark are well implemented in MORDA, and it does not degrade detectors' performance on nuScenes overall.

B. Impact of MORDA on D_{Real}^{Trg} (AI-Hub dataset)

To validate the efficacy of simulated features provided by MORDA in terms of previewing and indirectly learning about D_{Real}^{Trg} , we load the trained models from Sec. V-A and evaluate their performance on D_{Real}^{Trg} without further training.

1) *Real-target dataset*: A real-world driving dataset, AI-Hub is opted to represent D_{Real}^{Trg} given (1) its sensor data are collected from the real-target domain of this paper, South Korea where digital twin maps in MORDA ($D_{Syn}^{Src+Trg}$) are originated from. (2) Sensor suite and GT types are similar to nuScenes and MORDA, i.e., each frame contains five 1920×1200 multi-view images, one point cloud from 128-channel spinning LiDAR, and RTK GNSS data with 3D-BBox annotation frequency of 10 Hz.

2) *Pre-processing*: Tab. III summarizes the applied modifications. Format of AI-Hub dataset is converted to nuScenes style, following Sec. V-A.1. On top of that, we apply additional processing for fair experiments with Sec. V-A. (1) Only images from the front camera are used for 2D detection, and they are cropped to 1600×900. (2) We generated pseudo-2D-BBox labels exploiting pixel-level panoptic segmentation GT as they are not present in AI-Hub. Lastly, (3) we take 3D BBoxes only for four classes out of eight, i.e., car, truck,

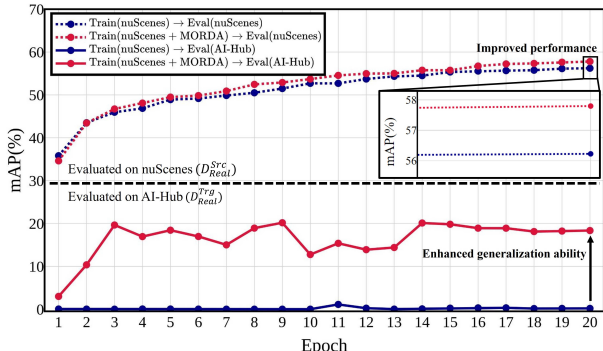


Fig. 5. Development of the mAP scores, training CenterPoint-Voxel (0.1m) over 20 epochs w/o (blue) and w/ (red) MORDA. The same models are evaluated on nuScenes (dotted) and AI-Hub (solid), respectively.

bus, and pedestrian, as they either have deviating labeling policies from nuScenes or have few instances (≤ 100). Note that all data of AI-Hub are used for validation, not training.

3) *Evaluation*: The right half of Tab. II shows detection scores of models evaluated on the unobserved AI-Hub dataset. As can be seen, detectors trained with MORDA exceed respective baselines by a large margin across modalities. For example, mAP gains of 6.3% for camera-based Faster-RCNN and 5.7% for LiDAR-based SSN are reported. This suggests that MORDA can provide simulated real-world experiences, assisting the adaptation of detectors and lessening reliance on real sensor data from D_{Real}^{Trg} .

In addition to the mentioned benefit above, we observe MORDA can assist in mitigating the generalization failure. Tab. II shows that the baseline CenterPoint family reports severe performance degradation under domain shift (nuScenes \rightarrow AI-Hub), meaning their class-wise AP and mAP scores on AI-Hub almost reach to zero regardless of backbone types. In contrast, when MORDA is included, mAP scores of all CenterPoint models get improved, meaning the observed generalization failures get alleviated. Especially, those with voxel backbones (0.1m and 0.075m) gain significant improvements in mAP (+18% and +22%). Fig. 5 explores this further and illustrates the development of mAP throughout entire training process with respect to the presence of MORDA. Notice that the model with MORDA achieves a substantial performance gap compared to the baseline on AI-Hub. In light of the analysis above, we conclude that MORDA is a well-constructed preview for D_{Real}^{Trg} and a useful regularization tool for generalization failure. Fig. 6 illustrates benefits of MORDA in this aspect.

C. Benchmark with Other Synthetic Datasets: 2D Detection

VKITTI2, SYNTHIA-AL, and SHIFT datasets are compared to MORDA in terms of mAP gains that respective datasets bring to Faster-RCNN trained on nuScenes.

1) *Pre-processing*: We use images from the front camera that all mentioned datasets above have in common. Next, we sample the datasets to match their frequencies as much as possible. That means MORDA, SYNTHIA-AL, and VKITTI2⁴ are downsampled to 2Hz. Although images

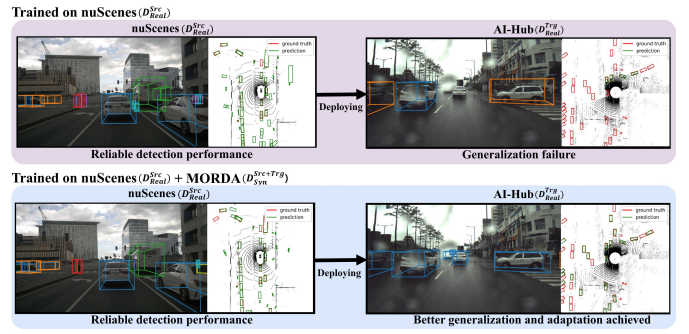


Fig. 6. Enhanced generalization performance of CenterPoint-Voxel (0.1m) with aid of MORDA. Camera images overlay predictions from the models.

TABLE IV
MAP GAINS IN FASTER-RCNN BY SYNTHETIC DATASET. DETECTION PERFORMANCE IS ASSESSED ON VALIDATION SPLIT OF NUSCENES.

Training Dataset	#Frame	mAP (%)
nuScenes	28K	27.3
nuScenes + VKITTI2	28K + 2.5K	27.0 (-0.3)
nuScenes + SYNTHIA-AL	28K + 7.3K	27.4 (+0.1)
nuScenes + SHIFT	28K + 30K	27.7 (+0.4)
nuScenes + MORDA (Ours)	28K + 3.7K	27.8 (+0.5)

of SHIFT dataset (discrete-shift) are already of 1 Hz, we downsample it by a factor of 5 due to its exceptional size (150K). Note that SHIFT is still the largest dataset after this downsampling, as shown in Tab. IV. 2D BBoxes of respective datasets are merged to nuScenes based on class labels.

2) *Training Details*: Faster-RCNN is trained on nuScenes and either of the synthetic datasets for all 10 detection classes, using MMDetection with default configuration.

3) *Evaluation*: Tab. IV presents mAPs of Faster-RCNNs trained with respective synthetic datasets along with the numbers of frames used for training. Our MORDA achieves 27.8%, surpassing the baseline and all the compared datasets. SHIFT shows a comparable mAP gain with ours, but it used 8x more frames than MORDA.

VI. CONCLUSIONS

For safety-critical AVs, DNNs need to overcome the performance degradation that occurs in unexperienced D_{Real}^{Trg} while maintaining performance on D_{Real}^{Src} . This paper proposed leveraging $D_{Syn}^{Src+Trg}$ where key characteristics of D_{Real}^{Src} and D_{Real}^{Trg} are fused. To showcase the efficacy, we generated a novel synthetic dataset, MORDA. Our comprehensive experiments demonstrate that MORDA could help DNNs adapt to D_{Real}^{Trg} , mitigating their dependency on real-world data without compromising performance on D_{Real}^{Src} .

Nevertheless, there is room for further research. Since only a simple concatenation of nuScenes and MORDA was used in this study, further performance enhancement on D_{Real}^{Trg} might be achieved by additionally incorporating modern UDA methods. Another direction for future work could be to identify which characteristics implemented in MORDA contributed to performance stability on D_{Real}^{Trg} by conducting an in-depth comparison with other synthetic datasets.

⁴The frequency of VKITTI2 is assumed to be the same as KITTI, as we could not find relevant information.

REFERENCES

[1] Z. Tian, C. Shen, H. Chen, and T. He, “FCOS: Fully convolutional one-stage object detection,” in *Proceedings of the IEEE/CVF International Conference on Computer Vision (ICCV)*, 2019.

[2] Z. Liu, Z. Wu, and R. Tóth, “SMOKE: Single-Stage Monocular 3D Object Detection via Keypoint Estimation,” in *Proceedings of the IEEE/CVF Conference on Computer Vision and Pattern Recognition Workshops*, 2020, pp. 996–997.

[3] Y. Wang, V. Guizilini, T. Zhang, Y. Wang, H. Zhao, and J. M. Solomon, “DETR3D: 3D Object Detection from Multi-view Images via 3D-to-2D Queries,” in *The Conference on Robot Learning (CoRL)*, 2021.

[4] A. H. Lang, S. Vora, H. Caesar, L. Zhou, J. Yang, and O. Beijbom, “PointPillars: Fast Encoders for Object Detection from Point Clouds,” in *Proceedings of the IEEE Conference on Computer Vision and Pattern Recognition*, 2019, pp. 12 697–12 705.

[5] X. Zhu, Y. Ma, T. Wang, Y. Xu, J. Shi, and D. Lin, “SSN: Shape Signature Networks for Multi-class Object Detection from Point Clouds,” in *Proceedings of the European Conference on Computer Vision*, 2020.

[6] T. Yin, X. Zhou, and P. Krähenbühl, “Center-based 3d object detection and tracking,” *CVPR*, 2021.

[7] G. Bang, K. Choi, J. Kim, D. Kum, and J. W. Choi, “RadarDistill: Boosting Radar-based Object Detection Performance via Knowledge Distillation from LiDAR Features,” 2024. [Online]. Available: <https://arxiv.org/abs/2403.05061>

[8] Y. Kim, J. Shin, S. Kim, I.-J. Lee, J. W. Choi, and D. Kum, “CRN: Camera Radar Net for Accurate, Robust, Efficient 3D Perception,” in *Proceedings of the IEEE/CVF International Conference on Computer Vision*, 2023, pp. 17 615–17 626.

[9] Z. Liu, H. Tang, A. Amini, X. Yang, H. Mao, D. Rus, and S. Han, “BEVFusion: Multi-Task Multi-Sensor Fusion with Unified Bird’s-Eye View Representation,” in *IEEE International Conference on Robotics and Automation (ICRA)*, 2023.

[10] J. Yan, Y. Liu, J. Sun, F. Jia, S. Li, T. Wang, and X. Zhang, “Cross Modal Transformer via Coordinates Encoding for 3D Object Detection,” *arXiv preprint arXiv:2301.01283*, 2023.

[11] J. Yang, S. Shi, Z. Wang, H. Li, and X. Qi, “ST3D: Self-training for Unsupervised Domain Adaptation on 3D Object Detection,” in *Proceedings of the IEEE/CVF Conference on Computer Vision and Pattern Recognition*, 2021.

[12] Jihani Yang, S. Shi, Z. Wang, H. Li, and X. Qi, “ST3D++: Denoised Self-training for Unsupervised Domain Adaptation on 3D Object Detection,” 2021. [Online]. Available: <https://arxiv.org/abs/2108.06682>

[13] S. R. Richter, Z. Hayder, and V. Koltun, “Playing for benchmarks,” in *IEEE International Conference on Computer Vision, ICCV 2017, Venice, Italy, October 22-29, 2017*, 2017, pp. 2232–2241. [Online]. Available: <https://doi.org/10.1109/ICCV.2017.243>

[14] Y. Cabon, N. Murray, and M. Humenberger, “Virtual KITTI 2,” 2020.

[15] A. Geiger, P. Lenz, and R. Urtasun, “Are we ready for autonomous driving? The KITTI vision benchmark suite,” in *2012 IEEE Conference on Computer Vision and Pattern Recognition*, 2012, pp. 3354–3361.

[16] J. Zolfaghari Bengar, A. Gonzalez-Garcia, G. Villalonga, B. Raducanu, H. Habibi Aghdam, M. Mozgov, A. M. Lopez, and J. van de Weijer, “Temporal coherence for active learning in videos,” in *Proceedings of the IEEE/CVF International Conference on Computer Vision (ICCV) Workshops*, Oct 2019.

[17] T. Sun, M. Segu, J. Postels, Y. Wang, L. Van Gool, B. Schiele, F. Tombari, and F. Yu, “SHIFT: A Synthetic Driving Dataset for Continuous Multi-Task Domain Adaptation,” in *Proceedings of the IEEE/CVF Conference on Computer Vision and Pattern Recognition (CVPR)*, June 2022, pp. 21 371–21 382.

[18] R. Xu, H. Xiang, X. Xia, X. Han, J. Li, and J. Ma, “OPV2V: An Open Benchmark Dataset and Fusion Pipeline for Perception with Vehicle-to-Vehicle Communication,” in *2022 International Conference on Robotics and Automation (ICRA)*. IEEE Press, 2022, p. 2583–2589. [Online]. Available: <https://doi.org/10.1109/ICRA46639.2022.9812038>

[19] H. Caesar, V. Bankiti, A. H. Lang, S. Vora, V. E. Lioung, Q. Xu, A. Krishnan, Y. Pan, G. Baldan, and O. Beijbom, “nuScenes: A multimodal dataset for autonomous driving,” in *CVPR*, 2020.

[20] S. R. Richter, V. Vineet, S. Roth, and V. Koltun, “Playing for Data: Ground Truth from Computer Games,” in *European Conference on Computer Vision (ECCV)*, ser. LNCS, B. Leibe, J. Matas, N. Sebe, and M. Welling, Eds., vol. 9906. Springer International Publishing, 2016, pp. 102–118.

[21] A. Gaidon, Q. Wang, Y. Cabon, and E. Vig, “Virtual worlds as proxy for multi-object tracking analysis,” in *Proceedings of the IEEE conference on Computer Vision and Pattern Recognition*, 2016, pp. 4340–4349.

[22] S. Ben-David, J. Blitzer, K. Crammer, A. Kulesza, F. C. Pereira, and J. W. Vaughan, “A theory of learning from different domains,” *Machine Learning*, vol. 79, pp. 151–175, 2010. [Online]. Available: <https://api.semanticscholar.org/CorpusID:8577357>

[23] M. K. Wozniak, M. Hansson, M. Thiel, and P. Jensfelt, “UADA3D: Unsupervised Adversarial Domain Adaptation for 3D Object Detection with Sparse LiDAR and Large Domain Gaps,” 2024. [Online]. Available: <https://arxiv.org/abs/2403.17633>

[24] P. Sun, H. Kretzschmar, X. Dotiwalla, A. Chouard, V. Patnaik, P. Tsui, J. Guo, Y. Zhou, Y. Chai, B. Caine, V. Vasudevan, W. Han, J. Ngiam, H. Zhao, A. Timofeev, S. Ettinger, M. Krivokon, A. Gao, A. Joshi, Y. Zhang, J. Shlens, Z. Chen, and D. Anguelov, “Scalability in Perception for Autonomous Driving: Waymo Open Dataset,” in *Proceedings of the IEEE/CVF Conference on Computer Vision and Pattern Recognition (CVPR)*, June 2020.

[25] T.-H. Vu, H. Jain, M. Bucher, M. Cord, and P. Pérez, “ADVENT: Adversarial Entropy Minimization for Domain Adaptation in Semantic Segmentation,” in *CVPR*, 2019.

[26] H. Zhao, R. T. des Combes, K. Zhang, and G. J. Gordon, “On Learning Invariant Representations for Domain Adaptation,” in *International Conference on Machine Learning*, 2019. [Online]. Available: <https://api.semanticscholar.org/CorpusID:174800477>

[27] F. Pan, I. Shin, F. Rameau, S. Lee, and I. S. Kweon, “Unsupervised Intra-domain Adaptation for Semantic Segmentation through Self-Supervision,” in *IEEE Conference on Computer Vision and Pattern Recognition (CVPR)*, 2020.

[28] Y. Yang and S. Soatto, “FDA: Fourier Domain Adaptation for Semantic Segmentation,” 2020. [Online]. Available: <https://arxiv.org/abs/2004.05498>

[29] A. Dosovitskiy, G. Ros, F. Codevilla, A. Lopez, and V. Koltun, “CARLA: An open urban driving simulator,” in *Proceedings of the 1st Annual Conference on Robot Learning*, ser. Proceedings of Machine Learning Research, S. Levine, V. Vanhoucke, and K. Goldberg, Eds., vol. 78. PMLR, 13–15 Nov 2017, pp. 1–16. [Online]. Available: <https://proceedings.mlr.press/v78/dosovitskiy17a.html>

[30] “MORAI Simulator,” <https://www.morai.ai/>, MORAI Inc.

[31] K. H. C. Manual, “Ministry of land,” *Transport and Maritime Affairs*, pp. p210–417, 2013.

[32] S. Ren, K. He, R. Girshick, and J. Sun, “Faster R-CNN: Towards Real-Time Object Detection with Region Proposal Networks,” *IEEE Transactions on Pattern Analysis and Machine Intelligence*, Jun 2017.

[33] K. Chen, J. Wang, J. Pang, Y. Cao, Y. Xiong, X. Li, S. Sun, W. Feng, Z. Liu, J. Xu, Z. Zhang, D. Cheng, C. Zhu, T. Cheng, Q. Zhao, B. Li, X. Lu, R. Zhu, Y. Wu, J. Dai, J. Wang, J. Shi, W. Ouyang, C. C. Loy, and D. Lin, “MMDetection: Open mmlab detection toolbox and benchmark,” *arXiv preprint arXiv:1906.07155*, 2019.

[34] M. Contributors, “MMDetection3D: OpenMMLab next-generation platform for general 3D object detection,” <https://github.com/open-mmlab/mmdetection3d>, 2020.